Grounding and Calving Cycle of Mertz Ice Tongue Revealed by Shallow Mertz Bank

Xianwei Wang[1,2], David M. Holland[1,3], Xiao Cheng[2,5] and Peng Gong[4,5]

1. Center for Global Sea Level Change, New York University Abu Dhabi. Abu Dhabi, United Arab Emirates.

2. State Key Laboratory of Remote Sensing Science, and College of Global Change and Earth System Science, Beijing Normal University. Beijing 100875, China.

3. Courant Institute of Mathematical Sciences, New York University. New York 10012, United States of America.

4. Ministry of Education Key Laboratory for Earth System Modeling, and Center for Earth System Science, Tsinghua University, Beijing, China 100084.

5. Joint Centre for Global Change Studies, Beijing, China.

Correspondence to: Xianwei Wang: *wangxianwei0304@163.com or* Xiao Cheng: *xcheng@bnu.edu.cn*

Abstract

A recent study, using remote sensing, provided evidence that a seafloor shoal influenced the 2010 calving event of the Mertz Ice Tongue (MIT), by partially grounding the MIT several years earlier. In this paper, we start by proposing a method to calculate Firn Air Content (FAC) around Mertz from seafloor-touching icebergs. Our calculations indicate the FAC around Mertz region as 4.87 ± 1.31 m. We then design an indirect method of using freeboard and sea surface height data extracted from ICESat/GLAS, FAC, and relatively accurate seafloor topography to detect grounding sections of the MIT between 2002 and 2008 and analyze the process of grounding prior to the calving event. By synthesizing remote sensing data, we point out that the grounding position was localized northeast of the Mertz ice front close to the Mertz Bank. The grounding outlines of the tongue caused by the Mertz Bank are extracted as well. From 2002 to 2008, the grounding area increased and the grounding became more pronounced. Additionally, the ice tongue could not effectively climb over the Mertz Bank in following the upstream ice flow direction and that is why MIT rotated clockwise after late 2002. Furthermore, we demonstrate that the area-increasing trend of the MIT changed little after calving (~36 km^2/a), thus allowing us to use remote sensing to estimate the elapsed time until the MIT can reground on and be bent by the shoal. This period is approximately 70 years. Our observations suggest that the calving of the MIT is a cyclical process controlled by the presence of the shallow Mertz Bank location and the flow rate of the tongue. This calving cycle also explains the cyclic variations in sea-surface conditions around the Mertz detected by earlier studies.

Keywords: Mertz Ice Tongue, firn air content, grounding, Mertz Bank, calving cycle.

1. Introduction

Surface-warming induced calving or disintegration of floating ice has occurred in Antarctica, such as the Larsen B ice shelf (Scambos et al., 2000, 2003; Domack et al., 2005; Shepherd et al., 2003). While surface or sub-surface melting has largely been recognized to contribute to floating ice loss in Antarctica (Depoorter et al., 2013), calving caused by interaction with the seafloor has not been widely considered. The Mertz Ice Tongue (MIT) was reported to have calved in 2010, subsequent to being rammed by a large iceberg, B-9B (Legresy et al. 2010). After the calving, the areal coverage of Mertz polynya, sea ice production and dense, shelf water formation in the region changed (Kusahara et al. 2011; Tamura et al. 2012). However, the iceberg collision may have only been an apparent cause of the calving as other factors had not been fully considered such as seafloor interactions (Massom et al., 2015; Wang. 2014). By comparing inverted ice thickness to surrounding bathymetry, and combining remote sensing analysis, Massom et al., (2015) considered that the seabed contact may have held the glacier tongue in place to delay calving by ~8 years. The interaction of the MIT with seafloor, the exact grounding location of the MIT before calving and the extent of grounding are still not well-known.

The MIT (66°S-68°S, 144°E-150°E, Fig. 1), located in King George V Land, East Antarctica, extended over 140 km from its grounding line to the tongue front and is approximately 30 km wide at the front (Legresy et al., 2004). Much field exploration has been conducted around Mertz and the increasing availability over the last decade of remote sensing, hydrographic surveying, and bathymetric data allows to investigate the mechanism of the ice tongue instability and calving. From satellite altimetry, a modest elevation change rate of 0.03 m/a (Pritchard et al., 2012) and a freeboard change rate of -0.06 m/a (Wang et al., 2014) were

57   found, which implied that the combined effects of surface accumulation and basal melt were not

58   dramatic for this ice tongue. Investigations of tidal effects, surface velocity, rift propagation, and

59   ice front propagation (Berthier et al., 2003; Frezzotti et al., 1998; Legresy et al., 2004;

60   Lescarmontier et al., 2012; Massom et al., 2010, 2015) have been conducted with an objective of

61   detecting underlying factors affecting the stability of the MIT. Grounding has been suggested as

62   a potential mechanism to affect the stability of the MIT by delaying calving (Massom et al.

63   2015). However, without highly accurate bathymetric data, it is impossible to carry out such a

64   study. Fortunately, In 2010, a new and high resolution bathymetry model, with a resolution of

65   100 m was released for the Terra Adelie and George V continental margin (Beaman et al., 2011),

66   and it has later been used to generate Bedmap-2 (Fretwell et al., 2013). This accurate data set

67   (Fig 3) provides an opportunity for better exploring seafloor shoals and their impacts on the

68   instability of the MIT. In this study, we focus on grounding events of the MIT from 2002 to 2008.

69   A method for grounding detection is proposed and grounding of the MIT before the calving is

70   investigated. A calving cycle of the MIT caused by grounding on seafloor shoal, Mertz Bank is

71   discussed as well.

72   **2. Data**

73   The primary data used to investigate grounding of the MIT in this study are elevation

74   data from Geoscience Laser Altimeter System (GLAS) onboard the Ice, Cloud and land

75   Elevation Satellite (ICESat) and the seafloor bathymetry data mentioned above. In this section,

76   the ICESat/GLAS and bathymetry data, as well as some preprocessing are introduced.

77   **2.1 ICESat/GLAS**

78   ICESat is the first spacebone laser altimetry satellite orbiting the Earth, launched by the

79   National Aeronautics and Space Administration (NASA) in 2003 (Zwally et al. 2002) with

80   GLAS as the primary payload onboard. ICESat/GLAS was operated in an orbit of ~600 km and

81   had a geographical coverage from 86°S to 86°N. ICESat/GLAS usually observed in nadir

82   viewing geometry and employed laser pulses of both 532 nm and 1064 nm to measure the

83   distance from the sensor to ground (Zwally et al. 2002). On the ground, ICESat/GLAS's

84   footprint covered an area of approximately 70 m in diameter, with adjacent footprints spaced by

85   ~170 m. The horizontal location accuracy of the footprint was approximately 6 m (Abshire et al.

86   2005). The accuracy and precision of ICESat/GLAS altimetry data were 14 cm and 2 cm

87   respectively (Shuman et al. 2006). ICESat/GLAS usually made two or three campaigns a year

88   from 2003 to the end of 2009, each campaign lasted for approximately one month. 15 different

89   types of data were produced for various scientific applications, named as GLA01, GLA02, …

90   GLA15. In this study, GLA12 data (elevation data for polar ice sheet) covering Mertz from

91   release 33 between 2003 and 2009 is used (Fig. 2).

92   **2.2 Seafloor Topography**

93   Detailed bathymetry maps are fundamental spatial data for marine science studies

94   (Beaman et al., 2003, 2011) and crucially needed in the data-sparse Antarctic coastal region

95   (Massom et al. 2015). Regionally, around Mertz, a large archive of ship track single-beam and

96   multi-beam bathymetry data from 2000 to 2008 were used to generate a high resolution Digital

97   Elevation Model (DEM) for which the spatial coverage can be found in Figs. 3(b) and 3(c). The

98   DEM product was reported to have a vertical accuracy of approximately 11.5 m (500 m depth)

99   and a horizontal accuracy of 70 m (500 m depth) in the poorest situation (Beaman et al. 2011).

100   As can be seen from Figs. 3(b) and 3(c), there is no bathymetry data under the MIT, which may

101   result in large uncertainty for seafloor interpolation. The oldest bathymetry data collected along

102   the margin of the MIT was from 2000 (Beaman et al. 2011). Additionally, around the Mertz ice

103 front, for both the east and west flanks, bathymetry data does exist. Since the ice front has a

104 width of ~34 km (Wang et al. 2014), the accuracy of seafloor DEM under the MIT varies

105 depending on distance to margin. Inside the 2000 boundary of the MIT, the closer to the dash-

106 dotted polygon (Figs. 6 and 7), the better accuracy the seafloor DEM. Outside of that boundary,

107 the quality of the seafloor DEM data is much better because of high density of single-beam or

108 multi-beam bathymetric measurements.

109   Around Antarctica, the seafloor topography data from Bedmap-2 was produced by

110 Fretwell et al. (2013) which adopted the DEM from Beaman et al. (2011). In this study,

111 Bedmap-2 seafloor topography data covering Mertz is employed to detect the contact between

112 seafloor and the MIT. Because of inconsistent elevation systems for ICESat/GLAS and the

113 seafloor topography data, the Earth Gravitational Model 2008 (EGM08) geoid (Pavlis et al. 2012)

114 with respect to World Geodetic System 1984 (WGS-84) ellipsoid is taken as reference. Since the

115 seafloor topography from Bedmap-2 is referenced to the so-called g104c geoid, an elevation

116 transformation is required and can be implemented through:

117 $E_{sf} = E_{seafloor} + gl04c_{to\_wgs84} - EGM2008$ (1)

118 where E_{sf} and $E_{seafloor}$ is the seafloor topography under the EGM08 and g104c geoid

119 respectively, $gl04c_{to\_wgs84}$ is the value needed to convert height relative to the gl04c geoid to

120 that under the WGS-84, and *EGM2008* is the geoid undulation with respect to the WGS-84.

121 **3. Methods**

122 **3.1 Grounding Detection Methods**

123   ICESat/GLAS data has been widely used to determine ice freeboard, or ice thickness,

124 since its launch in 2003 (Kwok et al., 2007; Wang et al., 2011, 2014; Yi et al., 2011; Zwally et

125 al., 2002, 2008). The methods we designed for grounding detection of the MIT using the

126   ICESat/GLAS data are introduced here. First, assuming a floating MIT, based on freeboard data

127   extracted in different observation dates, ice draft of the MIT is inverted. Next, ice bottom

128   elevation is calculated based on the inverted ice draft and the lowest sea-surface height. Finally,

129   the ice bottom is compared with seafloor bathymetry to detect ice grounding. The underlying

130   logic for grounding detection is that if the inverted ice bottom is lower than seafloor, we can

131   draw a conclusion that the ice tongue is grounding rather than floating.

132   The method for extracting a freeboard map using ICESat/GLAS from multiple campaigns

133   over the MIT was described in Wang et al. (2014). Without providing details, here we only

134   introduce it schematically. Four steps are included in freeboard map production for each of the

135   datasets from November 14, 2002, March 8, 2004, December 27, 2006 and January 31, 2008.

136   The first step involves data preprocessing, saturation correction, data quality control, and

137   tidal correction removal. The magnitude of the ICESat/GLAS waveform can become saturated

138   because of different gain setting, or high reflection from natural surfaces. Thus, saturated

139   waveforms with *i_satElevCorr* (i.e. an attribute from GLA12 data record) greater than or equal

140   to 0.50 m are ignored and only those measurements with *i_satElevCorr* less than 0.50 m are

141   corrected following the procedures in Wang et al. (2012, 2013). Additionally, measurements

142   with *i_reflctUC* greater than or equal to one are ignored. Furthermore, the tidal correction from

143   TPX07.1 tide model in GLA12 data record is removed to obtain estimates for the instantaneous

144   sea surface height. Finally, elevation data from ICESat/GLAS related to the WGS-84 ellipsoid

145   and EGM 08 geoid from 2003 to 2009 is available for subsequent use.

146   The second step is to derive sea-surface height according to each track and to calculate

147   freeboard for each campaign. Because of tidal variations near the MIT, surface elevations of the

148   MIT can vary as well. To derive sea-surface height from ICESat/GLAS and provide a reference

149 for freeboard calculation for different campaigns, the ICESat/GLAS data over the MIT within a

150 buffer region (with 10 km as buffer radius of MIT boundary in 2007) are selected and sea-

151 surface height is determined as the lowest elevation measurement along each track (Wang et al.

152 2014). Freeboard is then calculated by subtracting the corresponding sea-surface height from

153 elevation measurements of the MIT according to different tracks from the same campaign. Thus

154 freeboard data for different campaigns from 2003 to 2009 is obtained.

155   The third step is to relocate footprints using estimated ice velocity. ICESat observed the

156 MIT almost repeatedly along different tracks in different campaigns (Fig. 2). However,

157 observations from only one campaign cannot provide good coverage of the MIT. All

158 observations from 2003 to 2009 are combined together to produce a freeboard map of the MIT.

159 Fig. 2 shows the spatial coverage of ICESat/GLAS from 2003 to 2009 over Mertz, but the

160 geometric relation between tracks is not correct over the MIT because the tongue was fast

161 moving and observed in different years by ICESat. Regions observed in an earlier campaign

162 would move downstream later (Wang et al. 2014). For example, consider ICESat data from track

163 T31 from March 22, 2003 and T165 (Fig. 2) from November 1, 2003 respectively. Fig. 2 shows

164 that the distance between track T165 and T31 is ~7.5 km without accounting for ice advection

165 between observation dates. However because of the fast moving ice tongue, the distance of their

166 actual ground tracks on surface of the MIT should be longer because T165 was located upstream

167 and observed later. Thus footprints relocation using ice velocity is critical to obtain accurate

168 geometric relations among different tracks. The ice velocity data from Rignot et al. (2011)

169 generated from InSAR data from 2006 to 2010 is used to relocate the footprints of ICESat/GLAS.

170 The correct geospatial relations between observations from different campaigns can be achieved

171 on November 14, 2002, March 8, 2004, December 27, 2006, and January 31, 2008, through:

172 $$X = x + \sum_{i=1}^{n} v_{xi}\Delta t + v_{xm}t_m \qquad (2)$$

173 $$Y = y + \sum_{i=1}^{n} v_{yi}\Delta t + v_{ym}t_m \qquad (t_m = t_2 - t_1 - n\Delta t) \qquad (3)$$

174   where x and y are the horizontal positions directly from the ICESat measurements, and X

175 and Y are the horizontal positions after relocation respectively; v_x and v_y are the horizontal

176 components of the ice velocities; t_1 and t_2 are the start and end times; Δt is the time interval and

177 n indicates the largest integer time steps for time interval between t_1 and t_2; t_m is the residual

178 time; In this work, Δt is set as 10 days; v_{xi} and v_{yi} is derived from ice velocity field according

179 to different locations during relocation and may change in different time intervals.

180   Freeboard changes with time should be considered as well, but it is neglected because

181 comparison of freeboard from crossing tracks showed a slightly decreasing trend of -0.06 m/a on

182 average (Wang et al. 2014). The spatial distribution of freeboard data over the MIT for

183 November 14, 2002, is shown in Fig. 5(a).

184   The forth step is to interpolate the freeboard map using the relocated freeboard data from

185 the third step. Kriging interpolation in ArcGIS is selected in this study to produce freeboard

186 maps of the MIT because it can provide an optimal interpolation estimate for a given coordinate

187 location by considering the spatial relationships of a data set. With this method, freeboard maps

188 of the MIT are produced for November 14, 2002, March 8, 2004, December 27, 2006, and

189 January 31, 2008 respectively when the ice tongue outline can be delineated from Landsat

190 images.

191   Ice draft is calculated with Eq. (4) assuming hydrostatic equilibrium and using the lowest

192 sea-surface height E_{sea_level} as reference for the sea surface elevation.

193 $$\rho_w D = \rho_i(H_f + D - FAC) \qquad (4)$$

194   where D is the ice draft, i.e. vertical distance from the sea surface to the bottom of the ice;

195   H_f is the freeboard, i.e. the vertical distance from the sea surface to the top of the snow; ρ_w and

196   ρ_i are the densities of ocean water and ice, respectively. In this study, the ice and sea water

197   density are taken as 915 kg/m^3 and 1024 kg/m^3, respectively (Wang et al., 2014); FAC is the firn

198   air content which corresponds to the decrease in thickness (in meters) that occurs when the firn

199   column is compressed to the density of glacier ice, as defined in Holland et al., (2011) and

200   Ligtenberg et al. (2014).

201   The sea surface is taken as the lowest sea surface height (E_{sea_level}) and is derived from

202   the minimum of all sea surface heights from the different ICESat/GLAS tracks between 2003

203   and 2009 and amounts in our case to -3.35 m. For time varying sea-surface heights caused by

204   tides, the minimum sea-surface height can allow ice with a given draft to ground to the seafloor.

205   Then, the ice bottom elevation is calculated by considering the ice draft and the lowest sea-

206   surface height. Elevation difference of the ice bottom and the seafloor is calculated. A negative

207   value indicates that the ice bottom is lower than the seafloor, which suggests grounding.

208   The elevation of the underside (bottom) of the tongue E_{ice_bottom} is calculated from:

209     $E_{ice\_bottom} = E_{sea\_level} - D$ (5)

210   Similarly, the elevation difference of ice tongue bottom and seafloor is defined as E_{dif},

211   which can be calculated by:

212     $E_{dif} = E_{ice\_bottom} - E_{sf}$ (6)

213   where E_{sf} is the seafloor elevation as defined in Eq. (1).

214   **3.2. Firn Air Content Estimation Method**

215   The Antarctic ice sheet is covered by a dry, thick firn layer which represents an

216   intermediate stage between fresh snow and glacial ice, having varying density from Antarctic

217   inland to the coast (van den Broeke, 2008). The density and depth of the Antarctic firn layer has

218   been modeled (e.g., van den Broeke, 2008) using a combination of regional climate model output

219   and a steady-state firn compaction model. However, for ice thickness inversion, Firn Air Content

220   (FAC) is usually used to make the calculation convenient (Rignot and Jacobs. 2002). FAC is

221   defined as the decrease in thickness (in meters) that occurs when the firn column is compressed

222   to the density of glacier ice (Holland et al., 2011). Time-dependent FAC has also been modeled

223   by considering the physical process of the firn layer (e.g., Ligtenberg et al. 2014). For the MIT,

224   there are some in-situ measurements of snow thickness available from Massom et al. (2010) who

225   used a snow layer depth of 1 m to derive the thickness of surrounding multi-year, fast sea ice.

226   However on the surface of the MIT, no in-situ measurements of density or depth of firn layer are

227   available.

228   Because of different density and thickness of the firn layer on the top of an ice tongue, it

229   is challenging to simulate the density profile of the MIT without in-situ measurements as control

230   points. In this study, we use FAC extracted from adjacent seafloor-touching icebergs rather than

231   that from modeling to investigate the grounding of the MIT. The MIT may be composed of pure

232   ice, water, air, firn or snow that will influence the density of the ice tongue. However, if

233   assuming a pure ice density only to calculate ice mass, the thickness of MIT must be corrected

234   by the FAC. The FAC can be inferred from surrounding icebergs that are slightly grounded

235   under the assumption of hydrostatic equilibrium and known ice draft and freeboard.   It is,

236   however, critical to target and use icebergs that fulfil the condition of slight grounding. From

237   Smith (2011), icebergs can be divided into three categories based on bathymetry and seasonal

238   pack ice distributions: grounded, constrained, and free-drifting icebergs. Without pack ice, an

239   iceberg can be free-drifting or grounded. Free-drifting icebergs can move several tens of

240   kilometers a day, such as iceberg A-52 (Smith et al. 2007). Grounded icebergs can be heavily or

241   lightly anchored. Heavily grounded icebergs have firm contact with the seafloor and can be kept

242   stationary for a long time, such as iceberg B-9B (Massom. 2003). However, slightly grounded

243   icebergs may have less contact with the seafloor and can possibly move slowly under the

244   influence of ocean tide, ocean currents, or winds, but much slower than free-drifting icebergs.

245   The relation of grounded iceberg to the drifting velocity is not well-known. However, slowly

246   drifting or nearly stationary icebergs in open water are good indicators for slight grounding and

247   therefore are used to infer FAC.

248   Because of the heavily grounded iceberg B-9B to the east of the MIT blocking the

249   drifting of pack ice or icebergs from the east, icebergs located between B-9B and the MIT are

250   most likely generated from the Mertz or Ninnis glaciers. Some icebergs may be slightly

251   grounded as can be detected from remote sensing. We calculate the FAC from these slightly

252   grounded icebergs and later apply it to grounding event detection of the MIT. Around the MIT,

253   the locations of three icebergs ('A', 'B' and 'C') were investigated using MODIS and Landsat

254   images in austral summer of 2006 and 2008 respectively and shown in Fig. 4. Fortunately,

255   ICESat/GLAS observed these icebergs on February 23, 2006 (54th day of 2006) and February 18,

256   2008 (49th day of 2008) which allows us to analyze the behavior of these icebergs three-

257   dimensionally. Fig. 4a shows that icebergs 'A', 'B' and 'C' were almost stagnant and only

258   slightly changed their positions and orientation over two months (from 28 to 85 day of 2006).

259   Thus we can consider these icebergs slightly grounded. For these slightly grounded icebergs,

260   hydrostatic equilibrium should still apply, so the ice draft inverted from freeboard measurement

261   assuming hydrostatic equilibrium should be equal to the water depth. Based on this analysis, we

262   can take water depth as the draft to calculate the FAC.

263   Because only icebergs 'A' and 'C' were observed by track T1289 of ICESat/GLAS in

264   2006, the FAC is inverted using freeboard and water depth from bathymetry from both

265   icebergs(Figs. 3b, 3c, 4, and Table 1). However, the icebergs were not stationary, which

266   indicates that only some parts were slightly grounded. Therefore, only the top two largest

267   freeboard measurements of icebergs 'A' and 'C' from T1289 in 2006 are used to calculate the

268   FAC with Eq. (7) with a least-squares method under hydrostatic equilibrium.

269    $$FAC = H_{f\_k} + D_k - \frac{\rho_w}{\rho_i} D_k + \varepsilon_k \tag{7}$$

270   where k refers to the icebergs 'A' or 'C', H_f is the top two largest freeboard measurement of

271   each iceberg, D is the ice draft which is the same as sea water depth and is taken from the

272   seafloor bathymetry directly, ε is the residual of FAC.

273   Table 1 shows the freeboard of iceberg 'A' and 'C' from 2006 and seafloor bathymetry

274   for FAC inversion and grounding detection of icebergs 'A' and 'B' in 2008 (detailed freeboard

275   values for these icebergs can be found from S-Fig. 1). With the freeboard from 2006 and seafloor

276   bathymetry (Table 1), the FAC is calculated as 4.87±1.31 m. Icebergs 'A' and 'B' were observed

277   by the same track T1289 on February 18, 2008 and thus are taken to evaluate the grounding

278   detection by using the inverted FAC. From iceberg trajectories observed by remote sensing (Fig.

279   4b), we know, iceberg 'A' drifted away from its original position. Thus it was not grounded.

280   However, iceberg 'B' were kept rotating in this period without drifting away, indicating a slight

281   grounding. Such grounding status determined from remote sensing can also be detected with our

282   method since the elevation difference of the ice bottom and seafloor from Table 1 does clearly

283   indicate a slightly grounded iceberg 'B' and a floating iceberg 'A'. Thus, our FAC estimation

284   works well around Mertz.

285   FAC varies across the Antarctica ice sheet, usually decreasing from the interior to the

286   coast. For Mertz we obtain a FAC of 4.87 ± 1.31 m. Other studies, using a time variable approach,

287   modelled FAC values between 5 and 10 m (Ligtenberg et al. 2014) and in the absence of in-situ

288   measurements our estimate seems consistent, but there are some shortcomings which should be

289   further explored.

290   First, for FAC calculation, icebergs just touching the seafloor should be used in which

291   case the FAC calculated assuming hydrostatic equilibrium is the same as its actual value.

292   However, it is difficult to ascertain whether an iceberg is just touching the seafloor from remote

293   sensing images. The near stationary or slowly rotating icebergs detected with remote sensing

294   may be grounded more than just touching the seafloor, which may result in a inverted FAC

295   theoretically greater than its actual value. Thus, using this FAC value to detect grounding can

296   potentially lead to smaller grounding results. However, once a grounded iceberg or ice tongue is

297   detected using this FAC, the result is more convincing.

298   Second, limited observations from ICESat/GLAS may not catch the same and the thickest

299   section of a slight grounding iceberg. Because ICESat/GLAS observed only several times a year

300   on repeat tracks and icebergs were rotating slowly, the elevation profile in 2006 and 2008 along

301   the same track T1289 may not refer to the same ground surface. S-Fig. 1 shows the freeboard of

302   icebergs 'A', 'B' and 'C' derived from ICESat/GLAS from 2006 and 2008 respectively. By

303   comparing the freeboard of iceberg 'A' in 2006 (S-Fig. 1a), and 2008 (S-Fig. 1c), we find the

304   larger freeboard and the longer freeboard profile in 2006. Comparatively, the smaller freeboard

305   in 2008 may be caused by basal melting or observing a different portion of iceberg 'A' by

306   ICESat. Since the larger freeboard measured in 2006 indicates a high possibility of capturing the

307   thickest portion, it is reasonable to use it to invert the FAC. Additionally, icebergs 'A' and 'C'

308   did show a similar maximum freeboard (Table 1), which is another important reason to select the

309   measurements of 2006 for the inversion.

310   **4. Accuracy of Grounding Detection**

311   The accuracy of E_{dif} is critical to grounding detection of the MIT. From Eq. (1) to (6),

312   we find different components of error sources, such as from sea surface height determination, ice

313   draft, seafloor bathymetry, and elevation transformation. Meanwhile, the uncertainty of ice draft

314   is primarily depending on that of freeboard and FAC. Furthermore, the uncertainty of freeboard

315   is influenced by the footprint relocation and freeboard changing rates. Considering all that

316   mentioned above, the error sources of elevation difference E_{dif} can be synthesized by:

317    $$\Delta E_{dif} = \Delta E_{sl} + a(\Delta H_f + \Delta E_{re} + \Delta E_{fb_c} + \Delta FAC + \Delta E_{krig}) + \Delta E_{sf} + \Delta E_{trans} \qquad (8)$$

318   where $a = \frac{\rho_i}{\rho_w - \rho_i}$; Δ stands for error of each variable; ΔE_{dif} stands for the error of the final

319   elevation difference of ice bottom and seafloor; $\Delta E_{sl}, \Delta H_f, \Delta E_{re}, \Delta E_{fb\_c}, \Delta FAC, \Delta E_{sf}, \Delta E_{krig}$,

320   and ΔE_{trans} stand for errors caused by the sea surface height extraction, freeboard extraction,

321   freeboard relocation, freeboard changing rates, FAC calculation, seafloor bathymetry, kriging

322   interpolation and elevation system transformation, respectively.

323   The influence of elevation system transformation on final elevation difference can be

324   neglected. Based on the error propagation, the uncertainty of elevation difference E_{dif} can be

325   described by:

326    $$\varepsilon E_{dif} = \sqrt{(\varepsilon E_{sl})^2 + a^2[(\varepsilon H_f)^2 + (\varepsilon E_{re})^2 + (\varepsilon E_{fb_c})^2 + (\varepsilon FAC)^2 + (\varepsilon E_{krig})^2] + (\varepsilon E_{sf})^2}\,(9)$$

327   where ε indicates the uncertainty of each parameter.

328   **4.1 Uncertainty of Kriging Interpolation**

329   Fig. 5a shows the spatial distribution of freeboard data over the MIT used for grounding

330   detection from November 14, 2002. The spatial difference of the ICESat/GLAS data between

331   Fig. 2 and Fig. 5 is caused by the footprint relocation, after which the spatial geometry between

332   different tracks is reasonably correct. In the lower right of the Mertz ice front (Fig. 5a), the

333   crossing-track distance between T1289 and T165 is approximately 7 km. In these data gaps, the

334   freeboard data used for grounding detection is interpolated using kriging. Thus, knowing the

335   uncertainty of kriging interpolation is critical to the final grounding detection.

336   To investigate the uncertainty of kriging interpolation method, freeboard measurements

337   from ICESat/GLAS should be compared with the interpolated freeboard estimates. A testing

338   region with freeboard measurements is selected (dashed blue square in Fig. 5a, 7 km×7 km in

339   size). A freeboard map is first interpolated with the gray dots (Fig. 5a) using kriging. The

340   freeboard measurements (284 of green dots in Fig. 5a) are then compared with the interpolation

341   from the square. The spatial distribution and the histogram of freeboard difference derived by

342   subtracting the krigged freeboard from the freeboard derived from ICESat/GLAS are shown in

343   Fig. 5b.

344   The freeboard measurement varies from 31.6 m to 40.0 m with an average of 36.6 m.

345   However, the interpolated freeboard varies from 32.9 m to 39.6 m with an average of 35.9 m.

346   From the freeboard difference (Fig. 5b), we find that the interpolated freeboard shows similar

347   results compared with the freeboard derived from ICESat/GLAS. The interpolated freeboard has

348   an accuracy of -0.7±1.8 m indicating that the interpolated freeboard using kriging can reflect the

349   actual freeboard well.

350   **4.2 Grounding Detection Robustness**

351   Since the sea surface height is extracted from the ICESat/GLAS data track by track, we

352 use ± 0.15 m (Zwally et al. 2002) as the uncertainty of elevation data (εE_{sl}). Also from Wang et

353 al. (2014), we can find that the uncertainty of freeboard extraction (εH_f) was ± 0.50 m. From

354 Rignot et al. (2011), the error of the ice velocity ranged from 5 m/a to 17 m/a. Assuming that the

355 ice velocity varied by 17 m/a (an upper threshold), the relocation error horizontally could reach

356 ± 54 m when considering a three-year period. Wang et al. (2014) extracted the average slope of

357 the MIT along the ice flow direction as 0.00024. However, because of large crevasses on the

358 surface, we use 50 times of this value as a conservative estimate of the average slope. In this way,

359 we can estimate εE_{re} as ± 0.65 m when considering a three-year period. The annual rate of

360 freeboard changes from 2003 to 2009 was -0.06 m/a (Wang et al. 2014). Therefore, we consider

361 the freeboard stable over this period. However when combining data from different time periods,

362 εE_{fb_c} is estimated to be ± 0.18 m. From Beaman et al. (2011), considering the elevation

363 uncertainty at the worst situation when water depth reaches 500 m, εE_{g104c} is ± 11.5 m. Using Eq.

364 (9) and kriging interpolation, from the analysis from Section 4.1, 1.8 m is taken as the

365 uncertainty. Using all these errors above, we calculate the final uncertainty of the elevation

366 difference as ± 23 m.

367   From the calculations above, a less than -23 m E_{dif} indicates a robust grounding event.

368 However, if E_{dif} is greater than 23 m, grounding cannot be confirmed. E_{dif} between -23 m and

369 23 m corresponds to slight grounding or floating. We can also determine different contributions

370 of each separate factor to the overall accuracy. Seafloor bathymetry contributes the greatest part

371 and is the dominant factor affecting the accuracy of grounding detection.

372 **5. Grounding Detection Results**

373   The spatial distribution of the elevation difference E_{dif} and the outlines of the MIT from

374   2002 to 2008 are shown in Fig. 6. Since the moving trajectory of the Mertz ice front changed by

375   more than 40 degrees clockwise (Massom et al. 2015; Wang. 2014), a buffer region with radius

376   of 2 km (region between black and grey lines in Fig. 6) is introduced to investigate grounding

377   potential of the MIT. The freeboard in the buffer region is extrapolated using the kriging

378   interpolation method and the elevation difference is calculated. The elevation difference less than

379   46 m (twice the uncertainty of the elevation difference εE_{dif}) both inside and outside the outline

380   is extracted and the statistics are shown in Table 2. Since the uncertainty to determine a

381   grounding event is ± 23m, if some grids of the MIT have elevation difference E_{dif} less than -23

382   m, we can conclude that this section of the tongue is strongly grounded. The smaller the E_{dif}, the

383   more robust the grounding.

384   As illustrated in Table 2 and Fig 6, the minimum E_{dif} inside the MIT in 2002 was 11.9 m

385   and the minimum E_{dif} inside the MIT was less than -23 m after 2002. The minimum E_{dif} in the

386   buffer region were all less than -23 m from 2002 to 2008. This suggests that the MIT had

387   grounded on the shallow Mertz Bank at least since November 14, 2002. This result coincides

388   with the findings from Massom et al. (2015) who considered that the northwestern extremity of

389   the MIT started to touch a seafloor shoal in late 2002 to early 2003. Also, it would have been

390   difficult for the MIT to approach the buffer region (indicated with yellow to red colors in Fig. 6)

391   as the surrounding Mertz Bank gets shallower and steeper, suggesting substantive grounding

392   potentials. Inside the MIT, the minimum E_{dif} was just 11.9 m on November 14, 2002, which

393   indicates slight grounding. However on March 8, 2004, December 27, 2006, and January 31,

394   2008, the minimum E_{dif} reached -46.0 m, -52.3 m and -34.8m respectively, which indicates that

395   strong grounding occurred in some regions. From 2002 to 2008, more regions under the MIT had

396 E_{dif} less than 46 m, the area of which increased from 8 km^2 to 17 km^2. Additionally, the mean

397 of those E_{dif} less than 46 m gradually decreased from 28.8 m to 12.3m, according to which we

398 can conclude that the ice front became more firmly grounded as time passed on. Since the

399 grounding area increased from 8 km^2 to 17 km^2 (Table 2) and the mean of E_{dif} decreased, we

400 conclude that during the period from 2002 to 2008, the grounding of the northwest tip of the MIT

401 became more widespread.

402   Based on the calculated elevation difference, the grounding outlines of the MIT are

403 delineated for November 14, 2002, March 8, 2004, December 27, 2006 and January 31, 2008

404 respectively (Fig. 7). For the grounded part of the outlines in different years, the starting and

405 ending location and the perimeter are also extracted (Table 3), from which we conclude that the

406 length of the grounding outline on the Mertz Bank was only limited to a few kilometers. We find

407 that the lower right (northwest) section of the MIT was always grounded and grounding did not

408 occur in other regions (Fig. 6). The shallowest seafloor that the Mertz ice front touched was ~ -

409 290 m in November 2002. In 2004, 2006, and 2008, the lower right (northwest) of the MIT even

410 approached the contour of -220 m.

411 **6. Discussion**

412 **6.1 Area Changing Rate and ~70-year Calving Cycle of MIT**

413   Using Landsat TM/ETM+ images from 1989 to 2013, outlines of the MIT are extracted

414 manually. Assuming a fixed grounding line position, the area of the MIT over this period is

415 calculated. Using these data, from 1989 to 2007, an increasing are-change trend of the MIT was

416 obtained (from 5453 km^2 to 6126 km^2) in Fig. 8. However, the area of the MIT was almost

417 constant from 2007 to 2010, before calving. The largest area of the MIT was 6113 km^2 closest to

418 the calving event in 2010. After the calving, the area decreased to 3617 km^2 in November 2010.

419   The average area-change trend of the MIT from 1989 to 2007 was also obtained using a

420   least-squares method, corresponding to 35.3 km^2/a. However, after the calving a slightly higher

421   area-change trend of 36.9 km^2/a, was found (Fig. 8). On average, the area-change trend of the

422   MIT was approximately 36 km^2/a.

423   The surface dynamics of the MIT such as ice flow direction changes and middle rift

424   changes caused by grounding was analyzed by Massom et al. (2015). In the history of the MIT,

425   one or two large calving events were suspected to have happened between 1912 and 1956

426   (Frezzotti et al., 1998). Based on the interactions between the MIT and Mertz Bank suggested by

427   our observations and description below, it is likely that only one large calving event occurred

428   between 1912 and 1956. When the MIT touched Mertz Bank, the bank started to affect its

429   stability by bending it clockwise to the east, as can be found from velocity changes from

430   Massom et al. (2015). With continuous advection of the ice and flux input from the upstream, a

431   large rift from the west flank of the tongue would ultimately have to occur and could potentially

432   calve the MIT. A sudden length shortening of the MIT can be caused by such ice tongue calving

433   as indeed had happened in February, 2010. We also consider that even without a sudden collision

434   of iceberg B-9B in 2010, the MIT would eventually have calved because of the effect of the

435   shallow Mertz Bank.

436   When considering 6127 km^2 as the maximum area of the MIT and assuming a constant

437   area-changing trend of 36.9 km^2/a after 2010, the MIT will take approximately 68 years to calve

438   again. When assuming an area changing trend of 35.3 km^2/a as before 2010, the MIT will take a

439   little longer, approximately 71 years to calve. Therefore, without considering an accidental

440   collision with other large icebergs, the MIT is predicted to calve again in ~70 years. Because of

441   continuous advection of the ice from upstream and the fixed location of the shallow Mertz Bank,

442   the calving is likely repeatable and a cycle therefore exists.

443   After the MIT calved in February, 2010, the Mertz polynya size, sea-ice production, sea-

444   ice coverage and high-salinity shelf water formation changed as well. A sea-ice production

445   decrease of approximately 14-20% was found by Tamura et al. (2012) using satellite data and the

446   high-salinity shelf water export was reported to reduce up to 23% using a state-of-the-art ice-

447   ocean model (Kusahara et al. 2010). Recently, Campagne et al. (2015) pointed out a ~70-year

448   cycle of surface ocean condition and high-salinity shelf water production around the Mertz

449   through analyzing some reconstructed sea ice and ocean data over the last 250 years. They also

450   mentioned that this cycle was closely related to the presence and activity of the Mertz polynya.

451   However, the reason for this cycle was not fully understood.

452   From these findings addressed above and the MIT calving cycle we find that the calving

453   cycle of the MIT leads to the ~70-year cycle of surface ocean condition and high-salinity shelf

454   water production around the Mertz. Variations in length of the MIT will prevent sea ice drifting

455   from the east side to a variable degree. A long MIT contributes to maintain a large polynya

456   because sea ice from the east side cannot drift to the west side. The sea ice produced on the west

457   side is blown seaward by the katabatic wind and thereby maintains a polynya and stable sea ice

458   production. The sudden shortening of the MIT after a calving event therefore reduces the size of

459   Mertz Polynya formed by Antarctic katabatic winds, resulting in a lower sea-ice production and

460   further lessens high-salinity shelf water production. Therefore, the cycle of ocean conditions

461   around the Mertz found by Campagne et al. (2015) is likely dominated by the calving of the MIT.

462   Additionally, the 70-year cycle of the MIT calving coincides well with the change of surface

463   ocean condition around the Mertz which makes the explanation much more compelling.

6.2 Seafloor DEM

464

465   High accuracy seafloor is critical to the final success of the grounding detection.

466   According to our best knowledge, Beaman et al. (2011) provided the most accurate seafloor

467   DEM over the Mertz, so the seafloor DEM inside the dash-dotted polygon (Fig. 7) was kept and

468   the grounding detection was conducted there (Fig. 6). Additionally, the ice tongue continued to

469   advance out into the ocean, where the bathymetry observation density is good. From the results

470   shown in Fig. 6 all grounding sections of the MIT boundary were located outside of the 2000

471   boundary. Thus the analysis of the grounding detection near the ice front in 2002, 2004, 2006,

472   and 2008 is convincing. Inside the 2000 boundary, most of the grounding detection results were

473   above 100 m, indicating a floating status of the corresponding ice. Only abnormal seafloor

474   features higher than this seafloor DEM by more than 100 m could result in wide grounding

475   inside. Actually, no matter whether the MIT inside the 2000 boundary was grounded or not,

476   gradual grounding on the shallow Mertz Bank of the MIT since late 2002 is well supported by

477   observations and which we take as evidence to infer the primary cause of the instability of the

478   MIT.

6.3 Influence of Mertz Bank on MIT

479

480   Fig. 7 shows the extension line of the west flank in November, 2002, from which we can

481   find that if the MIT advected along the former direction, the ice flow would be seriously

482   obstructed when approaching the Mertz Bank. The shallowest region of the Mertz Bank has an

483   elevation of approximately -140 m and the MIT would have to climb the 140 m obstacle to cross

484   it. The shallow Mertz Bank would have caused strong grounding during the climbing. This

485   special feature of the seafloor shoal facing the MIT can further explain why the ice velocity

486   differed along the east and west flanks of the MIT before calving and why the ice tongue was

487 deflected clockwise to the east, as suggested by Massom et al. (2015). However, because of

488 sparsely-distributed bathymetric data in the Mertz region used in Massom et al. (2015), this

489 effect could not be easily seen. Here, from our grounding detection results and surrounding high-

490 accuracy bathymetry data, this effect is more clearly observed.

491 **7. Conclusion**

492   In this study, a method of FAC calculation from seafloor-touching icebergs around the

493 Mertz region is presented as an important element in understanding the MIT grounding. The

494 FAC around the Mertz is 4.87 ± 1.31 m. This FAC is used to calculate ice draft based on the sea

495 surface height and freeboard extracted from ICESat/GLAS and is performing well. A method to

496 extract the grounding sections of the MIT is described based on comparison of the inverted ice

497 draft assuming hydrostatic equilibrium with the seafloor bathymetry. The final grounding results

498 explain the dynamic behavior of the MIT. Previous work by Massom et al. (2015) has also

499 provided some evidence for seafloor interaction, in showing that the MIT front had an

500 approximate 280 m draft with the nearby seafloor as shallow as 285 m, suggesting the possibility

501 of grounding. In our work, we have provided ample detailed bathymetry and ice draft

502 calculations. Specifically, the ice bottom elevation of the MIT is inverted using the

503 ICESat/GLAS data and compared with seafloor bathymetry from 2002, 2004, 2006, and 2008

504 respectively. From these calculations we show conclusively that the MIT was indeed grounded

505 along a specific portion of its northwest tip over a limited region. We also point out that even

506 without collision by iceberg B-9B in early 2010 the ice tongue would eventually have calved

507 because of the ice advection from the upstream and the glacier flow increasingly diverted by the

508 obstructing seafloor shoal of the Mertz Bank.

509   From remote sensing images we are able to quantify the trend of area increase of the MIT

510 before and after the 2010 calving. While the area-increase trend of the MIT after calving was

511 slightly greater than that before, we use the averaged trend to estimate a timescale required for

512 the MIT to re-advance to the area of the shoaling bathymetry from its retreated, calved position.

513 Our estimate is ~70-years, which is remarkably consistent with Campagne et al. (2015) who

514 found a similar period for variations in sea surface conditions using seafloor sediment data. Thus,

515 the shoaling on the Mertz Bank combined with the rate of advancing of the MIT determines the

516 70-year repeat cycle. Also the calving cycle of the MIT explains the observed cycle of the sea-

517 surface conditions change well, which indicates that the calving of the MIT is the dominant

518 factor for the sea-surface condition change. Understanding the mechanism underlying the

519 periodicity of the MIT calving is important as the presence or absence of the MIT has a profound

520 impact on the sea ice and hence of the bottom water formation in the local region.

521 **Acknowledgements**

522   This research was supported by the Center for Global Sea Level Change (CSLC) of NYU

523 Abu Dhabi (Grant: G1204), the Open Fund of State Key Laboratory of Remote Sensing Science

524 (Grant: OFSLRSS201414), the National Natural Science Foundation of China (Grant: 41176163),

525 the China Postdoctoral Science Foundation (Grant: 2012M520185, 2013T60077) and

526 Fundamental Research Fund for the Central University. We are grateful to the Chinese Arctic

527 and Antarctic Administration, the European Space Agency for free data supply under project

528 C1F.18243, the National Snow and Ice Data Center (NSIDC) for the availability of the

529 ICESat/GLAS data (http://nsidc.org/data/order/icesat-glas-subsetter) and MODIS image archive

530 over the Mertz glacier (http://nsidc.org/cgi-bin/modis_iceshelf_archive.pl), British Antarctica

531 Survey   for   providing   Bedmap-2   seafloor   topography   data

532 (https://secure.antarctica.ac.uk/data/bedmap2/), the National Geospatial-Intelligence Agency for

533 publicly released EGM2008 GIS data (http://earth-

534 info.nga.mil/GandG/wgs84/gravitymod/egm2008/egm08_gis.html), and the USGS for Landsat

535 data (http://glovis.usgs.gov/). Fruitful discussions with M. Depoorter, P. Morin, T. Scambos and

536 R. Warner, and constructive suggestions from Editor Andreas Vieli and two anonymous

537 reviewers are acknowledged.

References

539 1. Abshire, J. B., Sun, X., Riris, H., Sirota, J. M., McGarry, J. F., Palm, S., ... & Liiva, P.

540   (2005). Geoscience laser altimeter system (GLAS) on the ICESat mission: on‐orbit

541   measurement performance. *Geophysical Research Letters*, 32(21).

542 2. Beaman, R. J., & Harris, P. T. (2003). Seafloor morphology and acoustic facies of the

543   George V Land shelf. *Deep Sea Research Part II: Topical Studies in Oceanography*,

544   50(8), 1343-1355.

545 3. Beaman, R. J., O'Brien, P. E., Post, A. L., & De Santis, L. (2011). A new high-resolution

546   bathymetry model for the Terre Adélie and George V continental margin, East Antarctica.

547   *Antarctic Science*, 23(01), 95-103.

548 4. Berthier, E., Raup, B., & Scambos, T. (2003). New velocity map and mass-balance

549   estimate of Mertz Glacier, East Antarctica, derived from Landsat sequential imagery.

550   *Journal of Glaciology*, 49(167), 503-511.

551 5. Campagne, P., Crosta, X., Houssais, M. N., Swingedouw, D., Schmidt, S., Martin, A., ...

552   & Massé, G. (2015). Glacial ice and atmospheric forcing on the Mertz Glacier Polynya

553   over the past 250 years. *Nature Communications*, 6.

554 6. Depoorter, M. A., Bamber, J. L., Griggs, J. A., Lenaerts, J. T. M., Ligtenberg, S. R. M.,

555   van den Broeke, M. R., & Moholdt, G. (2013). Calving fluxes and basal melt rates of

556   Antarctic ice shelves. *Nature*, 502(7469), 89-92.

557 7. Domack, E., Duran, D., Leventer, A., Ishman, S., Doane, S., McCallum, S., ... & Prentice,

558   M. (2005). Stability of the Larsen B ice shelf on the Antarctic Peninsula during the

559   Holocene epoch. *Nature*, 436(7051), 681-685.

560 8. Fretwell, P., Pritchard, H. D., Vaughan, D. G., Bamber, J. L., Barrand, N. E., Bell, R., ...

561   & Fujita, S. (2013). Bedmap2: improved ice bed, surface and thickness datasets for

562   Antarctica. *Cryosphere*, 7(1).

563 9. Frezzotti, M., Cimbelli, A., & Ferrigno, J. G. (1998). Ice-front change and iceberg

564   behaviour along Oates and George V Coasts, Antarctica, 1912-96. *Annals of Glaciology*,

565   27, 643-650.

566 10. Holland, P. R., Corr, H. F., Pritchard, H. D., Vaughan, D. G., Arthern, R. J., Jenkins, A.,

567   & Tedesco, M. (2011). The air content of Larsen ice shelf. *Geophysical Research Letters*,

568   38(10).

569 11. Kusahara, K., Hasumi, H. & Williams, G. D. (2011), Impact of the Mertz Glacier Tongue

570   calving on dense water formation and export. *Nature communications*, 2, 159.

571 12. Kwok, R. Cunningham, G. F., Zwally, H. J., & Yi, D. (2007). Ice, Cloud, and land

572   Elevation Satellite (ICESat) over Arctic sea ice: retrieval of freeboard. *Journal of

573   Geophysical Research,* 112, C12013, doi:10.1029/2006JC003978.

574 13. Legresy, B., Wendt, A., Tabacco, I. E., Remy, F., & Dietrich, R. (2004). Influence of

575   tides and tidal current on Mertz Glacier, Antarctica. *Journal of Glaciology*, 50(170), 427-

576   435.

577   14. Legresy, B., N. Young, L. Lescarmontier, R. Coleman, R.Massom, B. Giles, A. Fraser, R.

578   Warener, B. Galton-Fenzi, L. Testut, M. Houssais and G. Masse (2010), CRAC!!! in the

579   Mertz   Glacier,   Antarctica.

580   http://www.antarctica.gov.au/__data/assets/pdf_file/0004/22549/ml_402353967939815_

581   mertz_final_100226.pdf

582   15. Lescarmontier, L., Legrésy, B., Coleman, R., Perosanz, F., Mayet, C., & Testut, L. (2012).

583   Vibrations of Mertz glacier ice tongue, East Antarctica. *Journal of Glaciology*, 58(210),

584   665-676.

585   16. Ligtenberg, S., Kuipers Munneke, P., & Van Den Broeke, M. R. (2014). Present and

586   future variations in Antarctic firn air content. *The Cryosphere*, 8(5), 1711-1723.

587   17. Massom, R. A. (2003). Recent iceberg calving events in the Ninnis Glacier region, East

588   Antarctica. *Antarctic Science*, 15(02), 303-313.

589   18. Massom, R. A., Giles, A. B., Fricker, H. A., Warner, R. C., Legrésy, B., Hyland, G.,

590   Young, N., & Fraser, A. D. (2010). Examining the interaction between multi-year

591   landfast sea ice and the Mertz Glacier Tongue, East Antarctica: Another factor in ice

592   sheet   stability?   *Journal   of   Geophysical   Research*,   115,   C12027,

593   doi:10.1029/2009JC006083.

594   19. Massom, R. A., Giles, A. B., Warner, R. C., Fricker, H. A., Legrésy, B., Hyland, G., ... &

595   Young, N. (2015). External influences on the Mertz Glacier Tongue (East Antarctica) in

596   the decade leading up to its calving in 2010. *Journal of Geophysical Research: Earth*

597   *Surface*, 120(3), 490-506.

598   20. Pavlis, N. K., Holmes S. A., Kenyon, S. C., & Factor, J. K. (2012). The development and

599   evaluation of the Earth Gravitational Model 2008 (EGM2008), *Journal of Geophysical*

600   *Research*. 117, B04406, doi:10.1029/2011JB008916.

601   21. Pritchard, H. D., Ligtenberg, S. R. M., Fricker, H. A., Vaughan, D. G., Van den Broeke,

602   M. R., & Padman, L. (2012). Antarctic ice-sheet loss driven by basal melting of ice

603   shelves. *Nature*, 484(7395), 502-505.

604   22. Rignot, E., Mouginot, J. & Scheuchl, B. (2011), Ice flow of the Antarctic ice sheet.

605   *Science*, 333(6048), 1427-1430.

606   23. Rignot, E., & Jacobs, S. S. (2002). Rapid bottom melting widespread near Antarctic ice

607   sheet grounding lines. *Science*, 296(5575), 2020-2023.

608   24. Scambos, T. Hulbe, A., C. & Fahnestock, M. A. (2003). Climate-induced ice shelf

609   disintegration in the Antarctic Peninsula. *Antarctic Research Series*, 79, 79-92.

610   25. Scambos, T. Hulbe, A., C. Fahnestock, M. A. & Bohlander, J. (2000). The link between

611   climate warming and breakup of ice shelves in the Antarctic Peninsula. *Journal of*

612   *Glaciology*, 46(154), 516-530.

613   26. Shepherd, A., Wingham, D., Payne, T., & Skvarca, P. (2003). Larsen Ice Shelf has

614   progressively thinned. *Science*, 302(5646), 856-859.

615   27. Shuman, C. A., Zwally, H. J., Schutz, B. E., Brenner, A. C., DiMarzio, J. P., Suchdeo, V.

616   P., & Fricker, H. A. (2006). ICESat Antarctic elevation data: Preliminary precision and

617   accuracy assessment. *Geophysical Research Letters*, 33(7).

618   28. Smith, K. L., Robison, B. H., Helly, J. J., Kaufmann, R. S., Ruhl, H. A., Shaw, T. J., ... &

619   Vernet, M. (2007). Free-drifting icebergs: hot spots of chemical and biological

620   enrichment in the Weddell Sea. *Science*, 317(5837), 478-482.

29. Smith, K. L. (2011). Free-drifting icebergs in the Southern Ocean: an overview. *Deep Sea Research Part II: Topical Studies in Oceanography*, 58(11), 1277-1284.

30. Tamura, T., Williams, G. D., Fraser, A. D. & Ohshima, K. I. (2012). Potential regime shift in decreased sea ice production after the Mertz Glacier calving, *Nature communications*, 3, 826.

31. Van den Broeke, M. (2008). Depth and density of the Antarctic firn layer. Arctic, Antarctic, and Alpine Research, 40(2), 432-438.

32. Wang, X.W., Cheng, X., Gong, P., Huang, H. B., Li Z., & Li, X. W. (2011). Earth Science Applications of ICESat/GLAS: a Review. *International Journal of Remote Sensing*, 32, 23, 8837-8864, doi: 10.1080/01431161.2010.547533

33. Wang, X.W., Cheng, X., Gong, P., Shum, C. K., Holland, D.M., & Li, X.W. (2014). Freeboard and mass extraction of the disintegrated Mertz Ice Tongue with remote sensing and altimetry data. *Remote Sensing of Environment*, 144, 1-10.

34. Wang, X.W. (2014). Mertz ice tongue evolutions from satellite observed data, Postdoctoral Research Report, College of Global Change and Earth System Science, Beijing Normal University, China. doi: 10.13140/2.1.1006.1603

35. Wang, X., Cheng, X., Li, Z., Huang, H., Niu, Z., Li, X., & Gong, P. (2012). Lake water footprint identification from time-series ICESat/GLAS data. *IEEE Geoscience and Remote Sensing Letters*, 9(3), 333-337.

36. Wang, X., Gong, P., Zhao, Y., Xu, Y., Cheng, X., Niu, Z., ... & Li, X. (2013). Water-level changes in China's large lakes determined from ICESat/GLAS data. *Remote Sensing of Environment*, 132, 131-144.

643   37. Yi, D., Zwally, H.J., & Robbins, J. (2011). ICESat observations of seasonal and

644   interannual variations of sea-ice freeboard and estimated thickness in the Weddell Sea,

645   Antarctica (2003-2009). *Annals of Glaciology*, 52(57), 43-51.

646   38. Zwally, H. J., Schutz, B., Abdalati, W., Abshire, J., Bentley, C., Brenner, A., Buftona, J.,

647   Deziof, J., Hancocka, D., Hardinga, D., Herringg, T., Minsterh, B., Quinng, K., Palmi,

648   S., Spinhirnea, J., & Thomasj, R. (2002). ICESat's laser measurements of polar ice,

649   atmosphere, ocean, and land. *Journal of Geodynamics*, 34, 405-445.

650   39. Zwally, H. J., Yi, D., Kwok, R., & Zhao, Y. (2008). ICESat measurements of sea ice

651   freeboard and estimates of sea ice thickness in the Weddell Sea. *Journal of Geophysical*

652   *Research*, 113, C02S15, doi:10.1029/2007JC004284.

653

Figures

655
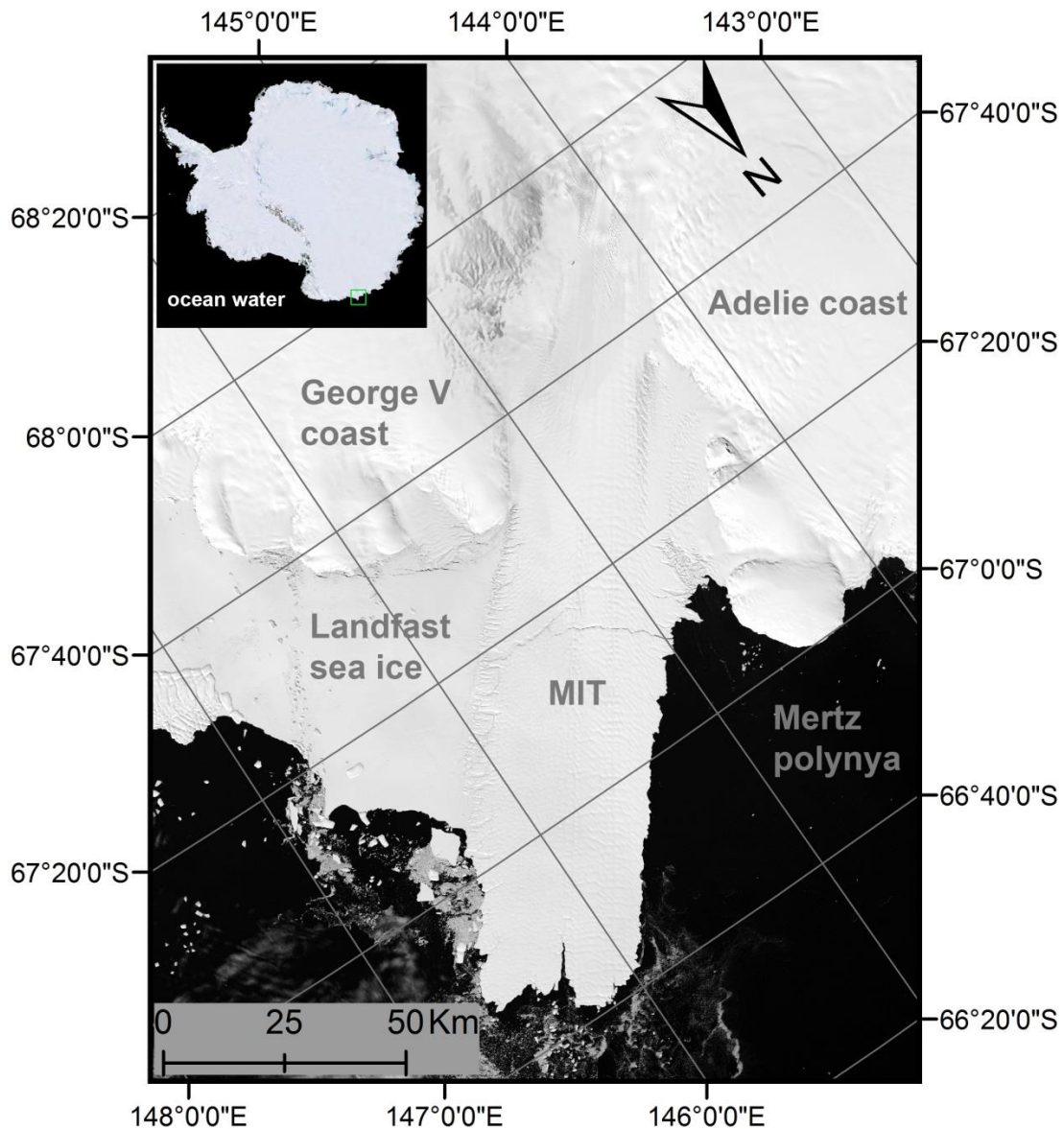
Figure 1. Mertz Ice Tongue (MIT), East Antarctica. Landfast sea ice is attached to the east flank

of the MIT and the Mertz Polynya is to the west. The background image corresponds to band 4

Landsat 7, captured on February 2, 2003. The green square found in the upper left inset indicates

the location of the MIT in East Antarctica. A polar stereographic projection with -71 °S as

standard latitude is used.

661

662
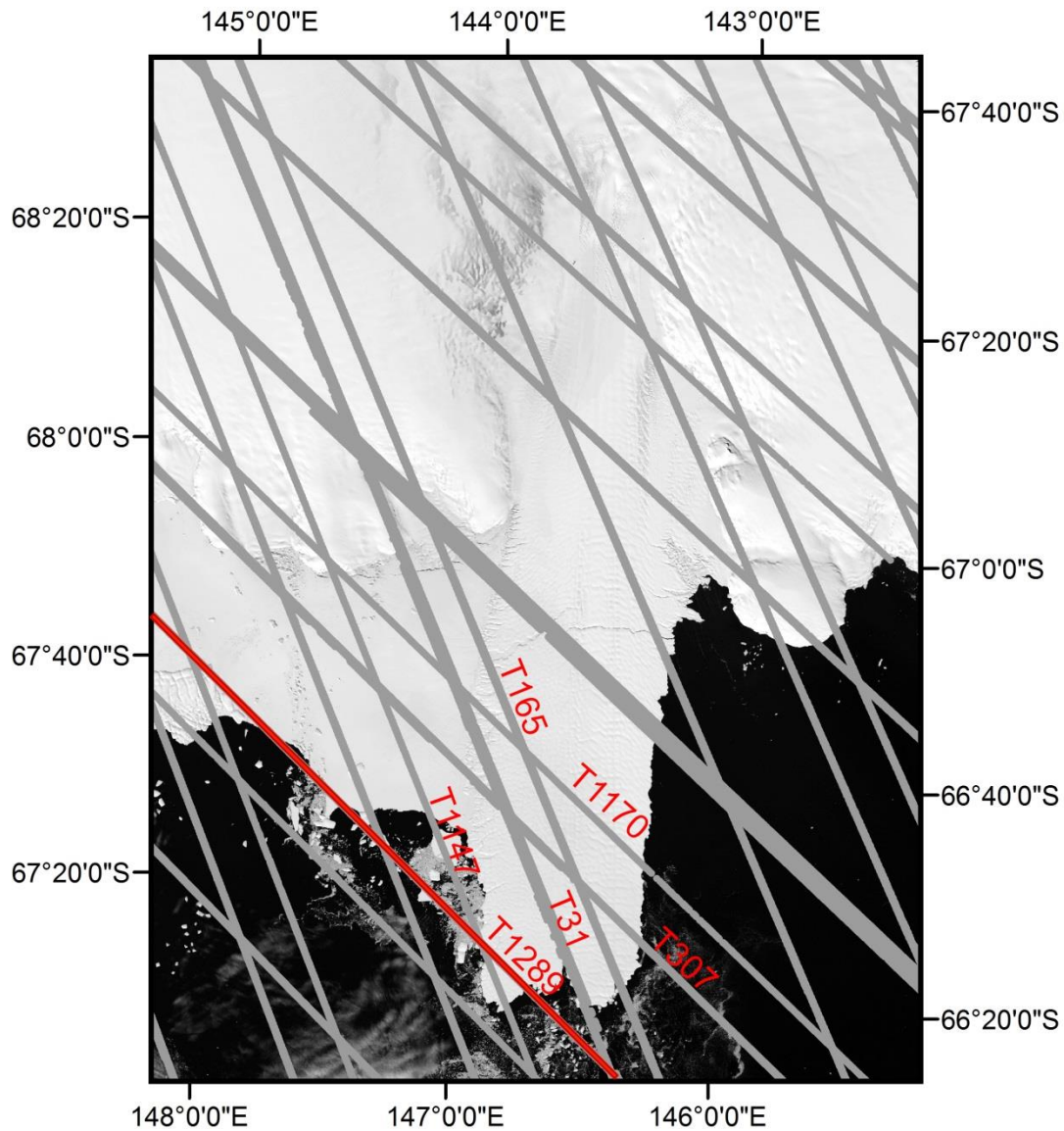
Figure 2. Spatial distribution of the ICESat/GLAS data from 2003 to 2009 covering the Mertz region. Ground tracks of ICESat/GLAS are indicated with gray lines. Track 1289 (T1289) is highlighted in red as is used in Fig. 4. The background image corresponds to band 4 Landsat 7, captured on February 2, 2003. A polar stereographic projection with -71 °S as standard latitude is used.

668

669

(a)

670

671

672

673   (b)

674

675

676   (c)
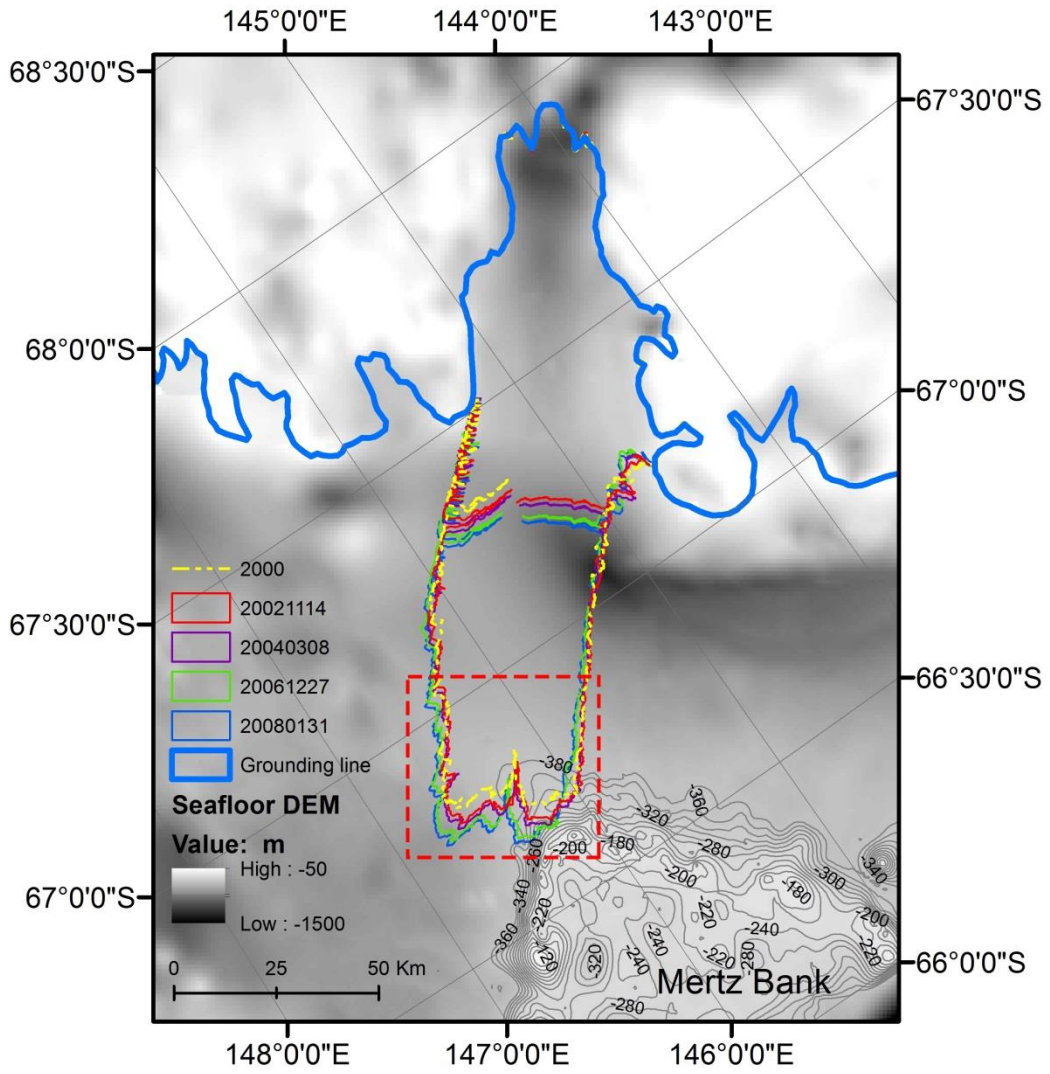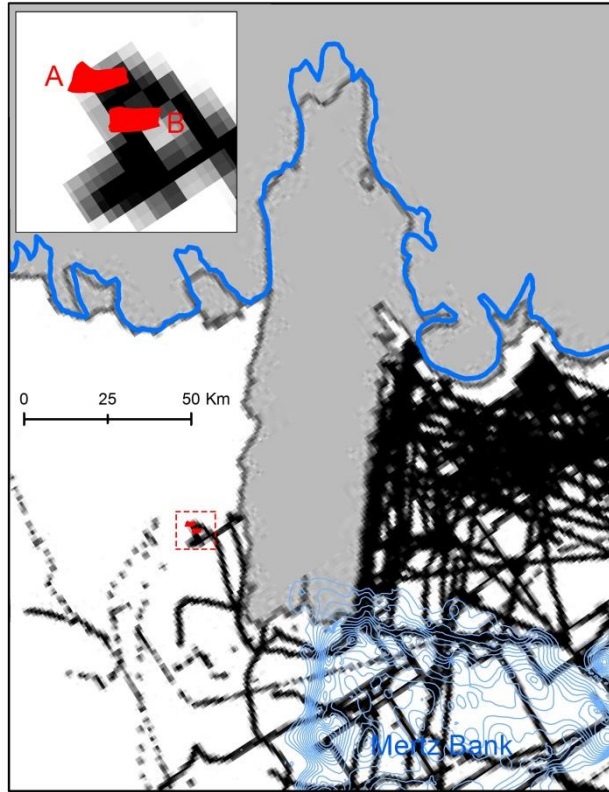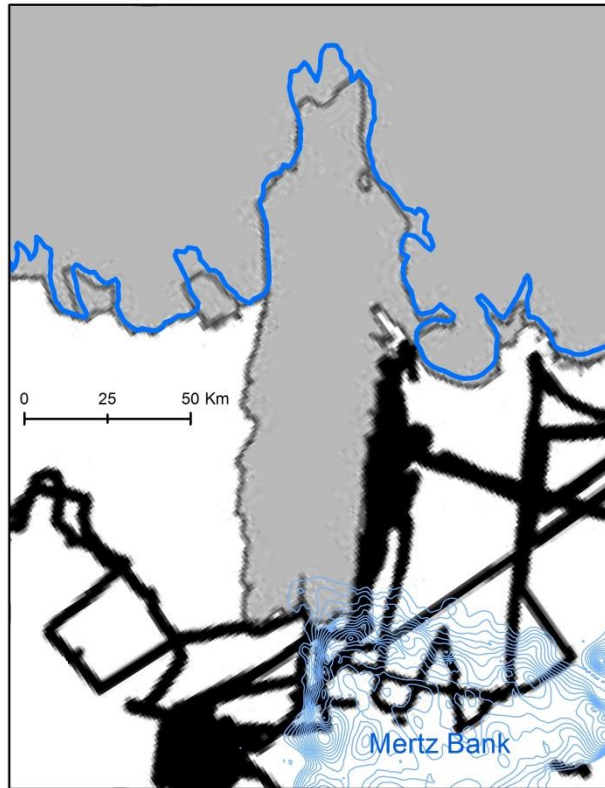
677

678   **Figure 3**. (a) Seafloor topography from bathymetry around Mertz and the outlines of the MIT

679   from 2002 to 2008 marked with the colored polygons for different years. The shallow Mertz

680   Bank is located in the lower right (northeast). The yellow dash-dotted line indicates the shape of

681   the MIT from January 25, 2000, which is used to identify the bathymetry gap under the ice

682   tongue. The dashed red inset box corresponds to the location of Figs. 6 and 7. (b) : multi-beam

683   bathymetry dataset coverage over the Mertz region. The embedded figure in the upper left is the

684   zoom in of the dashed red rectangle which shows the positions of icebergs 'A' and 'B' (polygon

685   filled in red) on February 19, 2008 (Fig. 4b). (c): single-beam bathymetry dataset coverage over

686   the Mertz region. The light blue polylines show the contours around the Mertz Bank and the

687   black dots are bathymetric measurement profiles. Both (b) and (c) are redrawn from Beaman et

688   al. (2011) because the original spatial coverage of the single and multi-beam bathymetry data is

689   not available. However, for being able to use the Figures from Beaman et al. (2011), we geo-

690   registered it and put the contour around the Mertz Bank and the location of icebergs used in the

691   text over it which illustrates the density of the bathymetry measurements. Through comparing

692   the grounding lines from (b) and (c), we can conclude that the geo-registration is successful as

693   the grounding line we obtained from the National Snow and Ice Data Center (NSIDC) coincides

694   with that from Beaman et al. (2011) well in most parts. This Figure is under a projection of polar

695   stereographic projection with -71 °S as standard latitude.

696

697
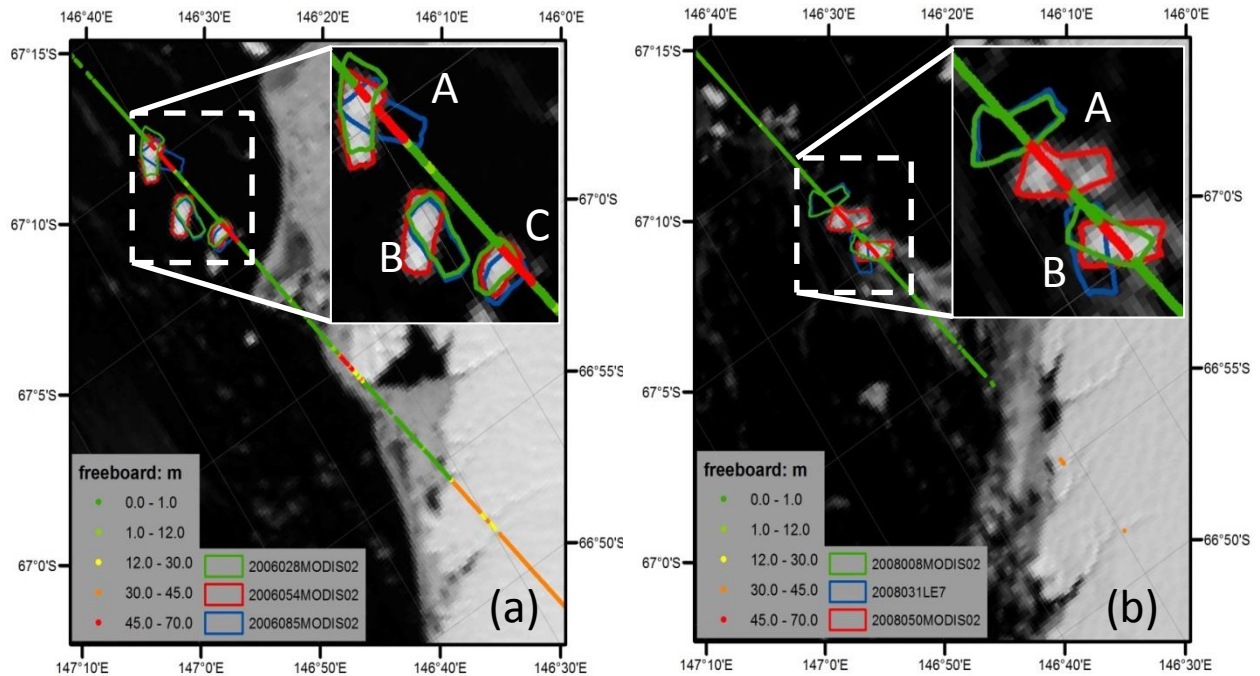
Figure 4. Freeboard extracted from Track T1289, ICESat/GLAS, the location of which can be found from Fig. 2 and Fig. 3(b). (a) and (b) show the freeboard extracted from the ICESat/GLAS date from February 23, 2006 (2006054) and February 18, 2008 (2008049) respectively. In each image, the positions of three icebergs (with name labeled as 'A', 'B' and 'C') closest to the ICESat/GLAS observation date are plotted with green, red and blue polygons respectively. The observation dates of remote sensing images are indicated with seven numbers (yyyyddd) in the legend. 'yyyyddd' stands for day 'ddd' in year 'yyyy'. 'MODIS02' and 'LE7' indicate that the images used to extract outlines of the icebergs are from MODIS and Landsat 7 ETM+, respectively.

707

708

709

710   (a)   (b)
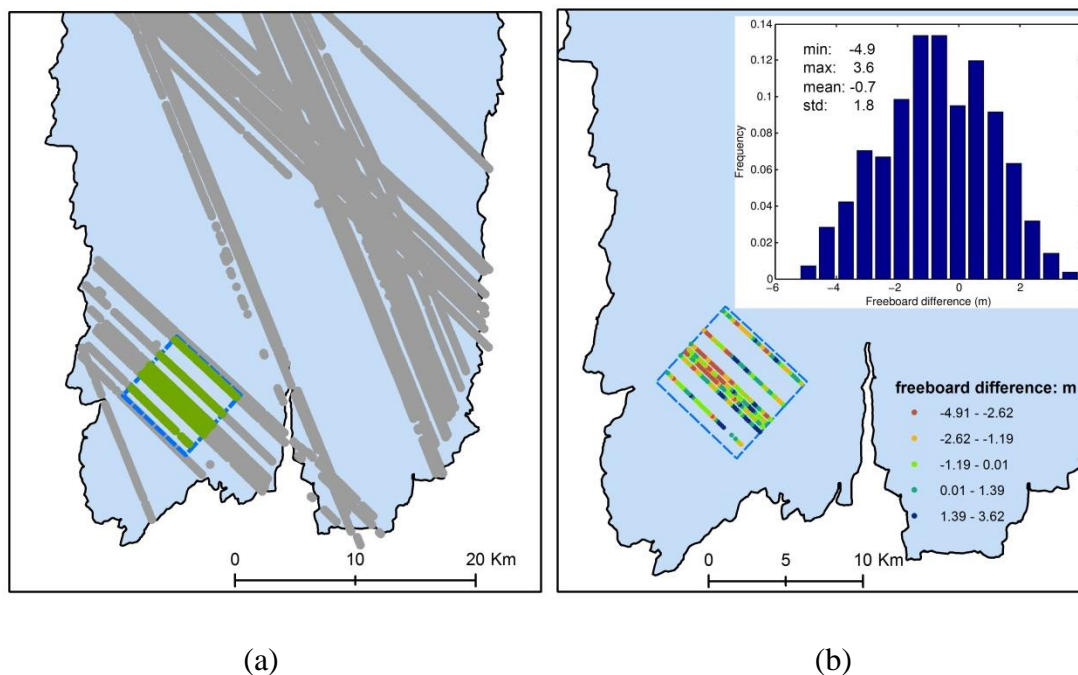
Figure 5. Evaluation of kriging interpolation method over the MIT using freeboard data derived

from the ICESat/GLAS data. (a) shows profile location of freeboard derived from the

ICESat/GLAS data after relocation over the MIT. The gray dots indicate the ICESat/GLAS data

used for interpolation using kriging method. The blue dashed square indicates the 7 km×7 km

region used to investigate the accuracy of kriging interpolation method. Inside the square, the

freeboard data marked with green dots are used to check the accuracy of the freeboard

interpolated with kriging. (b) is the freeboard comparison result derived by subtracting the

krigged freeboard from the freeboard derived from the ICESat/GLAS. The spatial distribution

and the histogram of the freeboard difference are shown in the lower left and upper right

respectively. The black polygon filled with light blue shows the boundary of the MIT on

November 14, 2002.

722

723

724   (a)   (b)

725

726   (c)   (d)
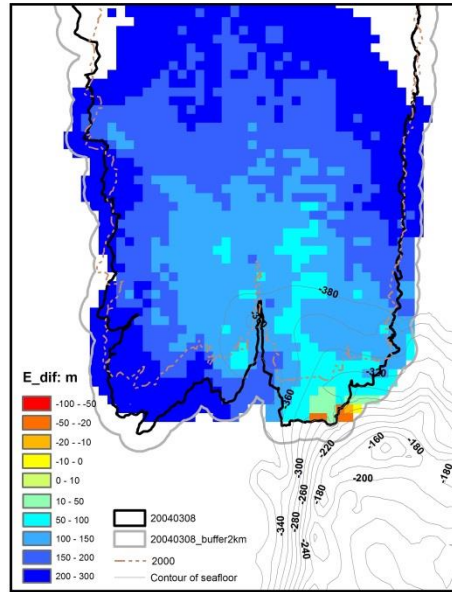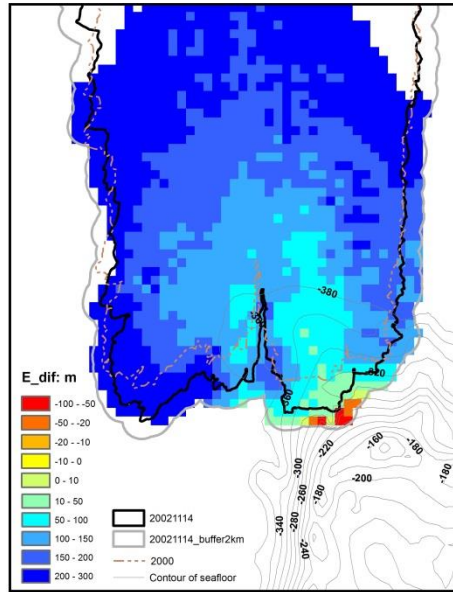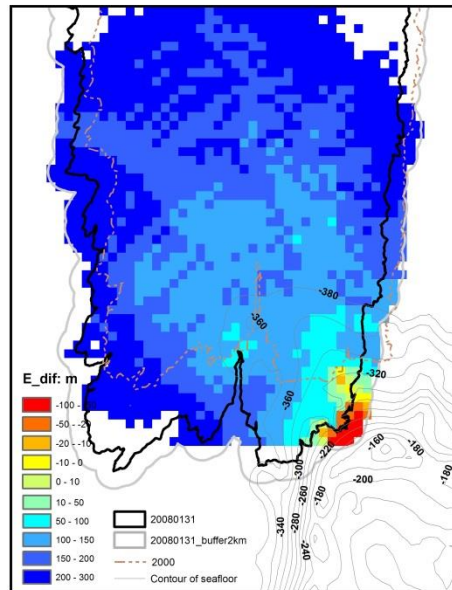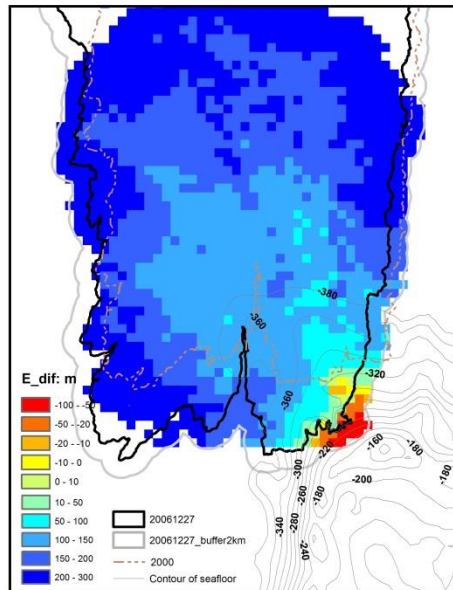
727 **Figure 6.** Elevation difference of Mertz ice bottom and seafloor topography. (a), (b), (c) and (d)

728 correspond to the elevation difference from November 14, 2002 , March 8, 2004, December 27,

729 2006, and January 31, 2008, respectively assuming hydrostatic equilibrium under the minimum

730 sea surface height -3.35 m . The contours at an interval of 20 m in the lower right indicate the

731 seafloor topography of the Mertz Bank. The solid black line indicates the boundary of the MIT

732 and the thick gray line outlines a buffer region of the boundary with 2 km as buffer radius. The

733 dash-dotted line indicates the shape of the MIT on January 25, 2000, which is used to identify

734 the bathymetry gap under the MIT. In the legend, the negative values mean that the ice bottom is

735 lower than the seafloor, which of course is impossible. Therefore, the initial assumption of a

736 floating ice tongue was incorrect in those locations (yellow to red colors), and the ice was

737 grounded. Regions with more negative values indicate heavier grounding inside the MIT or

738 grounding potential in the buffer region. Please note that no bathymetric data was available

739 under most of the ice tongue and for locations of the bathymetric data, please refer to Figs 3b and

740 3c.

741
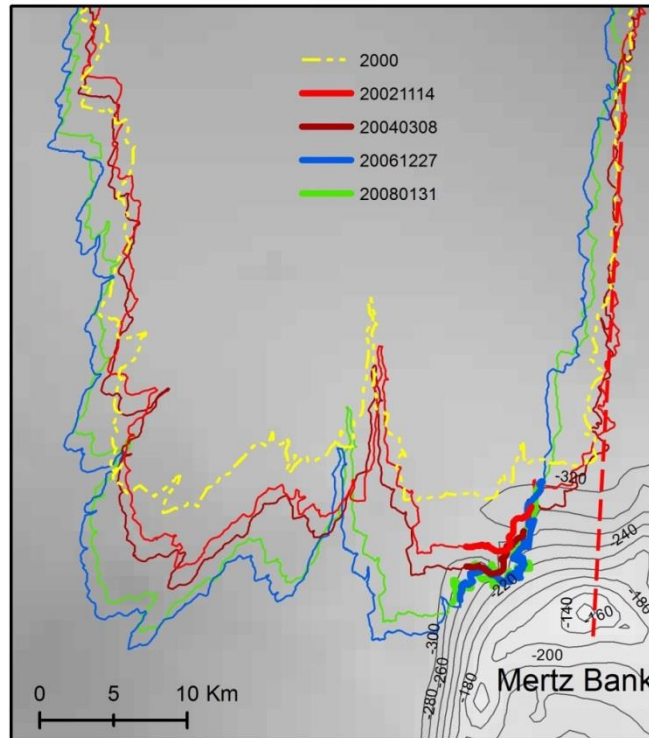
Figure 7. Digital Elevation Map (DEM) of seafloor around the Mertz and grounding section of the boundaries extracted from 2002 to 2008. The grounding sections of the MIT boundary from 2002, 2004, 2006 and 2008 are marked with thick red, purple, green and blue polylines respectively and the MIT boundaries are indicated with polygons with the same legend as in Fig. 3a. Additionally, the MIT boundary from 2000 indicated with dash-dotted yellow polygon is used to show the different quality of the seafloor DEM. Inside this polygon no bathymetry data was collected or used. The dashed red line indicates the 'extension line' of the west flank of the MIT on November 14, 2002, passing the shallowest region of the Mertz Bank (approximately -140 m).

751
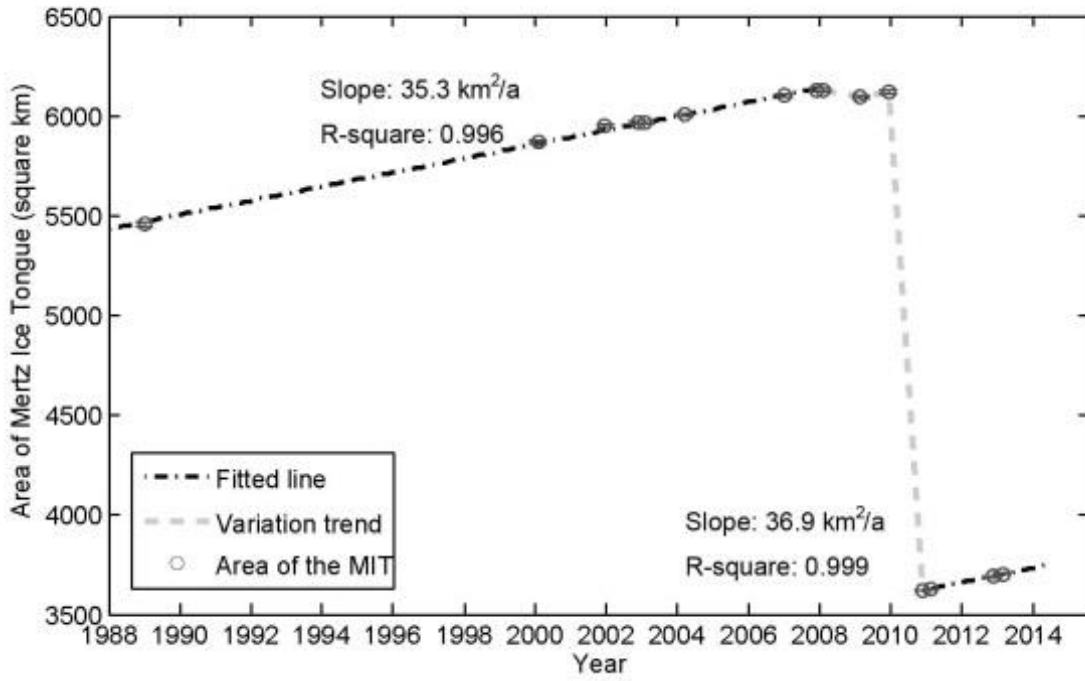
Figure 8. Average trend of the area change of the MIT. The area of the MIT is extracted from

the Landsat images from 1988 to 2013.

754

                  Tables

756 **Table 1**. Statistics of icebergs used to invert FAC with a least-square method and validation of

757 grounding iceberg detection using this FAC. Icebergs 'A', 'B' and 'C' are the same as what are

758 used in Fig. 4 and S-Fig 1. The measurements from icebergs 'A' and 'C' in February, 2006 are

759 used to derive the FAC with a least-squares method. However, the measurements from Icebergs

760 'A' and 'B' in 2008 are used for validation.

Icebergs	date	Latitude (°)	Longitude (°)	Freeboard (m)	Seafloor (m)	Sea Surface Height (m)	ε (m)	E_{dif} (m)
A	Feb 23, 2006	-67.1737	146.6595	66.88	-528.48	-1.92	0.89	
		-67.1752	146.6604	66.34	-527.01	-1.92	1.30	
C	Feb 23, 2006	-67.1085	146.6247	66.37	-505.84	-1.92	-1.25	
		-67.1100	146.6255	66.28	-507.08	-1.92	-1.01	
A	Feb 18, 2008	-67.1194	146.6303	58.88	-522.52	-2.08		69.14
		-67.1209	146.6311	59.58	-524.16	-2.08		64.88
B	Feb 18, 2008	-67.0906	146.6151	67.22	-500.92	-2.08		-22.45
		-67.0921	146.6159	66.10	-500.47	-2.08		-13.55

761

762 **Table 2**. Statistics of grounding grids inside the MIT or grounding potentials outside of the MIT

763 ('I': inside the thick black line, Fig. 6; Number in brackets indicates how many grids are located

764 inside the 2000 Mertz boundary; 'O': between the black and gray lines, Fig. 6) from November

765 14, 2002, March 8, 2004, December 27, 2006 and January 31, 2008 respectively. Each grid

766 covers an area of 1 km^2. The Mean, Minimum and Standard deviation is calculated without

767 considering those fallen inside the 2000 Mertz boundary and only include those out of the 2000

768 Mertz boundary with an elevation difference less than 46 m.

769

Elevation difference (subtracting seafloor from ice bottom)	2002-11-14		2004-03-08		2006-12-27		2008-01-31	
	I	O	I	O	I	O	I	O
23-46 (m)	9(3)	10(0)	6(0)	3(0)	10(1)	1(0)	10(3)	5(0)
0-23 (m)	2(0)	6(0)	1(0)	1(0)	9(0)	2(0)	4(0)	2(0)
<0 (m)	0(0)	8(0)	2(0)	5(0)	7(0)	21(0)	6(0)	18(0)
Mean (m)	28.8	9.8	15.8	-1.1	10.9	-41.9	12.3	-31.0
Minimum (m)	11.9	-81.5	-46.0	-44.5	-52.3	-102.8	-34.8	-103.0
Standard deviation (m)	9.2	36.8	29.6	31.4	24.7	37.6	27.3	38.0
Number of grids	8	24	9	9	25	24	17	25

770

771   **Table 3**. Statistics of grounding outlines of the MIT as shown with thick polylines in Fig. 7 from

772   November 14, 2002, March 8, 2004, December 27, 2006 and January 31, 2008 respectively

	2002-11-14	2004-03-08	2006-12-27	2008-01-31
Start location (°)	146.124 °E, 66.696 °S	146.155 °E, 66.681 °S	146.093 °E, 66.700 °S	146.088 °E, 66.699 °S
End location (°)	146.240 °E, 66.693 °S	146.256 °E, 66.683 °S	146.304 °E, 66.669 °S	146.292 °E, 66.668 °S
Perimeter (km)	7.0	6.4	24.7	20.9

773